Ferromagnetic transition and spin fluctuations in diluted magnetic semiconductors

Dinh-Hoi Bui,[1] Quoc-Huy Ninh,[2] Huu-Nha Nguyen,[3] and Van-Nham Phan[1,*]
[1]*Institute of Research and Development, Duy Tan University, 3 Quang Trung, 550000 Danang, Vietnam*
[2]*Natural faculty of science, Langson college of education, Chi Lang, 240000 Langson, Vietnam*
[3]*Department of Physics, HCMC University of Science, 227 Nguyen Van Cu, 700000 Ho Chi Minh City, Vietnam*

(Received 5 September 2018; revised manuscript received 3 December 2018; published 14 January 2019)

The magnetic properties over a wide range of temperatures in diluted magnetic semiconductors (DMSs) are discussed in the framework of the Kondo lattice model with magnetic impurity disorder. In the approach of dynamical mean-field theory, a set of self-consistent equations has been derived to specify single-particle Green functions. Analytical expressions of the static magnetic susceptibility and the B_{1g} channel Raman response are then delivered. Inspecting for signatures of an itinerant carrier density of states and magnetization, we have identified a stable ferromagnetic (FM) state at low temperature. With increasing temperature, thermal fluctuations diminish the ordered state and the system favors a paramagnetic (PM) phase. Tracking and tracing different model parameters, the FM-PM transition phase diagram has been constructed. Spin fluctuations in the PM state have been pointed out in the behaviors of the self-energies, the static magnetic susceptibility, and the Raman scattering. Analyzing the properties of the B_{1g} channel Raman response, we have attributed a formation of magnetic polarons in the PM state. The magnetic polaron scenario in a wide range of temperatures has been then intensively discussed. For the first time, both the static magnetic susceptibility and the B_{1g} Raman response have been combined together to discuss the magnetic properties in DMSs compactly based on the dynamical mean-field approach.

DOI: 10.1103/PhysRevB.99.045123

I. INTRODUCTION

Diluted magnetic semiconductors (DMSs) have attracted much attention because of their novel ferromagnetic (FM) properties and perspective applications in future spintronics [1,2]. Analyzing the FM state and its transition in the DMSs makes it possible to examine the physical properties due to interplay between semiconductor quantum structures and FM materials [1,2]. Due to a slight doping of magnetic ions into a semiconducting host (e.g., doping Mn in GaAs), the partially filled d-shell magnetic ions (Mn^{2+}) play dual roles of forming local magnetic moments and inducing the free carriers (holes) [3]. At low temperature, DMSs have been found to be FM [4,5]. The FM state is caused by the local exchange interaction between the impurities and the carriers, inducing a long-range effective ferromagnetic interaction between the impurity local moments [5–8]. Increasing temperature, the ordered state is suppressed and the system settles in the paramagnetic (PM) phase. The FM-PM transition scenario in DMSs has stimulated enormous attention [5–14].

To explain the FM-PM transition in DMSs, the formation of a magnetic cluster described in the sense of bound magnetic polaron states above the Curie temperature has been assumed [6,8,10–13]. As for decreasing temperature, the size of polarons increases until the magnetic clusters overlap through the whole sample at the FM-PM transition temperature. Using the lattice Monte-Carlo method adapted to a lattice spin-fermion model for DMSs, one can observe the magnetic clustered state above the Curie temperature [6]. In the meanwhile, to attribute the formation of magnetic clusters in the PM state, the polaron percolation theory has been widely utilized [8,11–13]. In our study, signatures of the FM-PM transition and the formation of magnetic polarons in the PM state in DMSs are investigated compactly in the framework of the single-site dynamical mean-field theory (DMFT). DMFT has been extensively used for investigating strongly correlated electron systems [15]. It is based on the fact that the self-energy depends only on the frequency in the infinite dimensional limit. The FM-PM transition temperature in DMSs has been examined by DMFT handling on a single-band model [5,7,16] or on a two-band model [14] but assuming that the effective medium is weakly linear dependent on the magnetization. Overcoming this assumption, in the present work, the FM-PM transition is studied in a signature of the static magnetic susceptibility function. Investigating a phase transition through its corresponding static susceptibility function is often a natural way in the literature [17]. In DMS, due to the strong compensation, the density of localized holes is much smaller than the density of Mn ions, leading to a polaronic picture in which a single hole polarizes a cloud of Mn spins, in other words, the polaron is formed around the carrier localized in the impurity band [10,18]. The DMFT is thus applicable to study the formation of the magnetic polaron in DMSs. The situation is similar to that of a lattice polaron, i.e., the case of an electron dressed by a phonon cloud, which has been profoundly considered within the single-site DMFT [19–23]. The single-site DMFT was also applied to discuss the lattice polaron scenario in connection with the magnetic polaron in the Holstein t-J model [24–26]. Of course, the

*Corresponding author: phanvannham@duytan.edu.vn

DMFT is essentially local, so intersite information, e.g., about the polaron size is difficult to obtain. Based on DMFT, the magnetic properties in DMSs in a wide range of temperatures are thus compactly discussed.

The Raman response has proven to be an effective tool for studying complex phase changes and especially in addressing the spin-disorder, magnetic polaron, and ferromagnetic states in low-carrier density magnetic systems [27–30]. In theoretical studies, the Raman scattering has been used to probe the magnetic polarons in the DMSs by the bound magnetic polaron theory [31–34]. Recently, the exchange interaction in a ferromagnetic semiconductor quantum well is also analyzed in a signature of the Raman scattering [35,36]. In the present work, the magnetic polaron formation in DMSs is indicated by studying the Raman scattering through the B_{1g} channel in the framework of DMFT. It is useful because there are no vertex corrections requiring the evaluation of the Raman B_{1g} channel response and it thus can be determined directly if one knows the single-particle spectral function of itinerant carriers derived from the present approach [37,38].

In DMSs, the doped magnetic ions act as an acceptor, so the main charge carrier in the DMSs is the hole. The holes are assumed to be able to hop in the lattice that creates the quasiparticle band and, for simplicity, it is often modeled by the tight-binding approximation [39,40]. We assume that the doped magnetic ions are randomly substituted in the cation sites, so in the lattice, only a fraction of lattice sites are occupied by the magnetic impurities and the remaining sites are nonmagnetic. The local spin exchange is valid only on the magnetic impurity sites. Due to the substitution, a local potential for the charge carriers at the magnetic impurity sites is needed to be taken into account. This situation looks similar to doped manganites in which rare-earth ions are replaced by divalent alkaline ions [41–44]. By adapting the DMFT, the model including all the above complex scatterings has been used to describe the spin dynamics in paramagnetic DMSs [45]. In the same manner, we present here a solution of DMFT adapting to the model showing the magnetic properties in DMSs in a whole range of temperatures. At low temperatures, by analyzing the density of states (DOS) of the itinerant carriers and examining the magnetization and self-energies, the system has been pointed out to stabilize in a FM state. Due to the thermal fluctuations, the FM state is suppressed and the FM-PM transition temperature can be evaluated in the divergence of the static magnetic susceptibility, and the FM-PM transition phase diagram is then constructed. In the PM state, the spin fluctuation properties in the system are discussed in the signatures of the susceptibility function and the Raman response. The B_{1g} channel Raman response shows us the potential formation of a magnetic polaron in PM state, which is diminished with increasing temperature. The magnetic polaron in DMSs, therefore, is discussed based on a well-known theoretical method, the DMFT. Moreover, the PM-PM transition in DMSs in the signature of the static magnetic susceptibility function is also addressed in the framework of the DMFT.

The present paper is organized as follows. In Sec. II, we present a microscopic Hamiltonian essentially applied for the DMS materials and its DMFT solution. Section III outlines an analytic calculation of the static spin susceptibility function based on the results of the DMFT in the previous section. In Sec. IV, we present the numerical results and their discussions. A summary and conclusion are presented in the last section.

II. MODEL AND DYNAMICAL MEAN-FIELD THEORY

Taking into account both the magnetic coupling between the local magnetic moment with a spin of the itinerant carriers and the potential arising due to the random magnetic ions in DMSs, we introduce in the following an appropriate microscopic Hamiltonian in the tight-binding approximation:

$$\mathcal{H} = -t \sum_{\langle i,j\rangle\sigma} c^{\dagger}_{i\sigma} c_{j\sigma} + 2J \sum_{i} \alpha_i \mathbf{S}_i \mathbf{s}_i - \mu \sum_{i} n_i + \sum_{i} U \alpha_i n_i, \tag{1}$$

where $c^{\dagger}_{i\sigma}$ and $c_{i\sigma}$ are the creation and annihilation operators for an itinerant carrier with spin σ at lattice site i, respectively. t is the nearest-neighbor-hopping integral, which is scaled with the spatial dimension d as $t = t^*/2\sqrt{d}$ in the infinite dimensional limit [15]. In the analytical calculations below, $t^* = 1$ is taken as the unit of energy. $\mathbf{S}_i$ is the magnetic impurity moment at lattice site i, while $\mathbf{s}_i = \sum_{ss'} c^{\dagger}_{is} \boldsymbol{\sigma}_{ss'} c_{is'}/2$ is the spin of the itinerant carriers ($\boldsymbol{\sigma}$ are the Pauli matrices), the second term in Eq. (1) indicates the magnetic coupling in DMSs. In the present work, the magnetic exchange is considered in the Ising-type, i.e., only the z component of the magnetic moment is accounted. Indeed, the essential features of the magnetic and electronic properties in DMSs do not depend on whether the exchange is of Ising- or Heisenberg-type coupling [7,46–48]. We treat this simplified type to make our further simple calculation in the next section. The last term addresses the potential arising when the lattice site is occupied by magnetic ions. U is the strength of the magnetic disorder and is mapped onto the difference in the local potential, which splits energetically in favor of the lattice site with and without magnetic doping. In general, the disorder is site-dependent, however, in our work, we handle the bulk system by approximating to infinite dimensions, thus the disorder can be introduced in average and is considered as a kind of the diagonal disorder. That diagonal disorder has been intensively studied in the literature by the DMFT [15,49–53].

In the Hamiltonian in Eq. (1), we have also included α_i as a classical variable that takes the value of either 1 or 0 if site i is occupied or unoccupied by a magnetic ion, respectively. The appearance of α ensures that the spin exchange and the magnetic disorder arise only on the lattice sites that are occupied by the magnetic ions. If x is the doping number of the magnetic ions in DMSs, α is distributed like a binary function:

$$\mathcal{P}(\alpha) = (1-x)\delta(\alpha) + x\delta(1-\alpha). \tag{2}$$

In the case of $\alpha_i = 1$ for all i, the first three terms in the Hamiltonian illustrate the Kondo lattice model [5]. In the Hamiltonian, μ is the chemical potential that is introduced to control carrier doping.

The Hamiltonian given in Eq. (1) has been discussed in the framework of DMFT but only in the PM state [45]. In the following, we address the application of DMFT to the model in Eq. (1) in a wide range of temperatures so the spin dependence of the single-particle Green's function is explicitly considered from the beginning. Moreover, we also point out some functionals that would be used in the next section to evaluate the static magnetic susceptibility function.

We now present a DMFT application to the Hamiltonian in Eq. (1). The DMFT is a nonperturbative local theory, the self-energies driven from the time-dependent mean-field function must be thus local or momentum independent. The DMFT, therefore, is exact in the infinite space dimensional limit. The local Green function of itinerant carriers with spin σ can be determined via the equation

$$G_\sigma(i\omega_n) = \int d\varepsilon \rho(\varepsilon) \frac{1}{i\omega_n - \varepsilon + \mu - \Sigma_\sigma(i\omega_n)}, \tag{3}$$

where $\omega_n = (2n+1)\pi T$ is the Matsubara frequency at temperature T, $\Sigma_\sigma(i\omega_n)$ is the self-energy, and $\rho(\varepsilon)$ is the noninteracting DOS of the itinerant carriers. In the infinite dimensional hypercubic lattice, it has a Gaussian form: $\rho(\varepsilon) = \exp(-\varepsilon^2)/\sqrt{\pi}$.

The local Green function must coincide with the Green function determined within the effective single impurity embedded in the dynamical mean-field medium. In this issue, one obtains

$$G_\sigma(i\omega_n) = \int d\alpha \mathcal{P}(\alpha) \frac{\delta \ln \mathcal{Z}^\alpha_{\rm eff}}{\delta \mathcal{G}^{-1}_\sigma(i\omega_n)}, \tag{4}$$

where $\mathcal{Z}^\alpha_{\rm eff}$ is the partition function of the effective problem, which depends on whether a site is doped by the magnetic ions or not and $\mathcal{G}_\sigma(i\omega_n)$ is the Green function of the effective medium. Within the effective single-site problem, the partition function is

$$\mathcal{Z}^\alpha_{\rm eff} = {\rm Tr} \int D c^\dagger_\sigma D c_\sigma e^{-S^{[s,\alpha]}_{\rm eff}}. \tag{5}$$

The trace in Eq. (5) is taken over all possible values of s, and the action for this effective problem $S^{[s,\alpha]}_{\rm eff}$ is given by

$$S^{[s,\alpha]}_{\rm eff} = -\int_0^\beta d\tau \int_0^\beta d\tau' \sum_\sigma c^\dagger_\sigma(\tau) \mathcal{G}^{-1}_\sigma(\tau - \tau') c_\sigma(\tau') + \int_0^\beta d\tau \sum_\sigma [Js\sigma + U]\alpha c^\dagger_\sigma(\tau) c_\sigma(\tau), \tag{6}$$

where $\mathcal{G}_\sigma(\tau - \tau')$ is the time-dependent Green function of the effective medium. It acts as the bare Green function of the effective problem. Using a Fourier transformation, the effective action in Eq. (6) can be written as

$$S^{[s,\alpha]}_{\rm eff} = -\sum_{n\sigma} \bar{c}_{n\sigma} \left[\mathcal{G}^{-1}_\sigma(i\omega_n) - (Js\sigma + U)\alpha\right] c_{n\sigma}, \tag{7}$$

with $\bar{c}_{n\sigma}$ and $c_{n\sigma}$ being the Grassman variables. With the help of Eq. (7), one can calculate exactly the partition function in Eq. (5), it reads

$$\mathcal{Z}^\alpha_{\rm eff} = {\rm Tr}\left\{ 2 \exp\left[\sum_{n\sigma} \ln \frac{\mathcal{G}^{-1}_\sigma(i\omega_n) - (Js\sigma + U)\alpha}{i\omega_n} \right] \right\}. \tag{8}$$

Then one obtains an explicit expression of the local Green function from the effective single impurity solution in Eq. (4):

$$G_\sigma(i\omega_n) = \sum_{\alpha s} \frac{W_{\alpha s}}{\mathcal{G}^{-1}_\sigma(i\omega_n) - (Js\sigma + U)\alpha}. \tag{9}$$

Note here that the expression of the distribution function in Eq. (2) has been used. In Eq. (9), $W_{\alpha s}$ ($\alpha = \{0, 1\}$) act as the weight factors, which explicitely read

$$W_{0s} = \frac{2(1-x)}{\mathcal{Z}^0_{\rm eff}} \exp\left[\sum_{n\sigma} \ln \frac{\mathcal{G}^{-1}_\sigma(i\omega_n)}{i\omega_n} \right] \tag{10}$$

and

$$W_{1s} = \frac{2x}{\mathcal{Z}^1_{\rm eff}} \exp\left[\sum_{n\sigma} \ln \frac{\mathcal{G}^{-1}_\sigma(i\omega_n) - (Js\sigma + U)}{i\omega_n} \right]. \tag{11}$$

Note that the weight factors $W_{\alpha s}$ are not simply a number. They are functionals of the local Green function. This is an important feature of the DMFT that gives nontrivial contributions to the response functions of the system [54–56]. In our calculation, the magnetic doping x in DMSs has appeared in the weight factors. To close a set of self-consistent equations, one notes that the local Green function also satisfies the Dyson equation

$$G^{-1}_\sigma(i\omega_n) = \mathcal{G}^{-1}_\sigma(i\omega_n) - \Sigma_\sigma(i\omega_n). \tag{12}$$

From Eqs. (3), (9), and (12), we obtain a set of self-consistent equations allowing us to determine the self-energies $\Sigma_\sigma(i\omega_n)$ and then the local Green function of the itinerant carriers numerically. Starting from some initial values for $\Sigma_\sigma(i\omega_n)$, the local Green function $G_\sigma(i\omega_n)$ in Eq. (3) and then $\mathcal{G}_\sigma(i\omega_n)$ in Eq. (12) are determined. With the new $\mathcal{G}_\sigma(i\omega_n)$, one finds a new local Green function $G_\sigma(i\omega_n)$ from Eq. (9). Then, using Eq. (12), the self-energies $\Sigma_\sigma(i\omega_n)$ are recalculated and the self-consistent process is restarted until a convergence is achieved.

III. STATIC MAGNETIC SUSCEPTIBILITY

To detect the FM and analyze magnetic fluctuations in the PM state, in this section, we examine the static magnetic susceptibility for the model given in the Hamiltonian (1). Based on the DMFT equations in the previous section, we shall derive an analytical expression of the static magnetic susceptibility function. Note here that the magnetic susceptibility function is valid only in PM state and it diverges at the magnetic transition point. The static magnetic susceptibility in momentum space is defined by

$$\chi(\mathbf{q}) = -\sum_{ij} e^{-i\mathbf{q}(\mathbf{R}_i - \mathbf{R}_j)} \chi(i, j), \tag{13}$$

where the magnetic correlation function in the real space $\chi(i, j)$ reads

$$\chi(i, j) = \langle(\delta n_{i\uparrow} - \delta n_{i\downarrow})(\delta n_{j\uparrow} - \delta n_{j\downarrow})\rangle. \quad (14)$$

Here we have defined the density fluctuation operator at a site i with spin σ: $\delta n_{i\sigma} = n_{i\sigma} - \langle n_{i\sigma}\rangle$. The correlation function in Eq. (14) can be rewritten as

$$\chi(i, j) = \sum_{\sigma\sigma'} \chi_{\sigma\sigma'}(i, j)\sigma\sigma', \quad (15)$$

where $\chi_{\sigma\sigma'}(i, j) = \langle\delta n_{i\sigma}\delta n_{j\sigma'}\rangle$. The correlation functions $\chi_{\sigma\sigma'}(i, j)$ can be obtained by differentiating the Green function respected to the external magnetic field h and then taking the zero limit of the field [54–56], i.e.,

$$\chi_{\sigma\sigma'}(i, j) = -T^2 \sum_n \frac{dG_{ii,\sigma}(i\omega_n)}{dh_{j\sigma'}}\bigg|_{h=0}. \quad (16)$$

Following a feature developed in calculating the susceptibility functions previously in Ref. [41,43], we derive an expression of the static magnetic susceptibility function

$$\chi(\mathbf{q}) = -T^2 \sum_n \chi(\mathbf{q}, i\omega_n), \quad (17)$$

where

$$\chi(\mathbf{q}, i\omega_n) = R_n(\mathbf{q})\left[2 - \frac{1}{2}\sum_{\alpha s\sigma}\left(\frac{\partial\Sigma_\sigma(i\omega_n)}{\partial W_{\alpha s}}\right)_{G, W_{\overline{\alpha s}}} \sigma\gamma_{\alpha s}(\mathbf{q})\right]. \quad (18)$$

Here,

$$R_n^{-1}(\mathbf{q}) = [\chi_0(\mathbf{q}, i\omega_n)]^{-1} + \frac{1}{2}\sum_\sigma\left(\frac{\partial\Sigma_\sigma(i\omega_n)}{\partial G_\sigma(i\omega_n)}\right)_W, \quad (19)$$

and $\chi_0(\mathbf{q}, i\omega_n) = \sum_{\mathbf{k},\sigma} G_\sigma(\mathbf{k}+\mathbf{q}, i\omega_n)G_\sigma(\mathbf{k}, i\omega_n)/2$ is the bare particle-hole susceptibility. $\gamma_{\alpha s}(\mathbf{q})$ term in Eq. (18) can be determined in a matrix identity

$$\widehat{\gamma}(\mathbf{q}) = \widehat{Q}^{-1}(\mathbf{q})\widehat{P}(\mathbf{q}), \quad (20)$$

where the matrices $\widehat{Q}(\mathbf{q})$, $\widehat{P}(\mathbf{q})$ have the following elements:

$$\begin{aligned} Q_{\alpha s,\alpha' s'}(\mathbf{q}) &= \delta_{\alpha\alpha'}\delta_{ss'} - A_{\alpha s,\alpha' s'}(\mathbf{q}) \\ &\quad + \frac{1}{2}\sum_{n\sigma\sigma'} R_n(\mathbf{q})\left(\frac{\partial\Sigma_\sigma(i\omega_n)}{\partial W_{\alpha' s'}}\right)_{G, W_{\overline{\alpha' s'}}} B^{\sigma'}_{\alpha s,n}(\mathbf{q})\sigma\sigma', \\ P_{\alpha s}(\mathbf{q}) &= 2\sum_{n\sigma} R_n(\mathbf{q})B^{\sigma}_{\alpha s,n}(\mathbf{q})\sigma. \end{aligned} \quad (21)$$

Here we have introduced the following notations:

$$\begin{aligned} A_{\alpha s,\alpha' s'}(\mathbf{q}) &= \sum_{n\sigma}\frac{\partial W_{\alpha s}}{\partial\mathcal{G}_\sigma^{-1}(i\omega_n)}\left(\frac{\partial\Sigma_\sigma(i\omega_n)}{\partial W_{\alpha' s'}}\right)_{G, W_{\overline{\alpha s}}}, \\ B^{\sigma}_{\alpha s,n} &= \left[\left(\frac{\partial\Sigma_\sigma(i\omega_n)}{\partial G_{\sigma'}(i\omega_n)}\right)_W - \frac{1}{G_\sigma^2(i\omega_n)}\right]\frac{\partial W_{\alpha s}}{\partial\mathcal{G}_\sigma^{-1}(i\omega_n)}. \end{aligned} \quad (22)$$

The derivatives in Eqs. (18)–(22) can be calculated explicitly. From the result of the local Green function in Eq. (9) and expressions of the weight factors in Eqs. (10) and (11), we straightforwardly obtain

$$\left(\frac{\partial\Sigma_\sigma(i\omega_n)}{\partial W_{\alpha s}}\right)_{G, W_{\overline{\alpha s}}} = \frac{1}{S_{n\sigma}\left[\mathcal{G}_\sigma^{-1}(i\omega_n) - (J\sigma s + U)\alpha\right]}, \quad (23)$$

$$\left(\frac{\partial\Sigma_\sigma(i\omega_n)}{\partial G_\sigma(i\omega_n)}\right)_W = \frac{1}{G_\sigma^2(i\omega_n)} - \frac{1}{S_{n\sigma}}, \quad (24)$$

$$\frac{\partial W_{\alpha s}}{\partial\mathcal{G}_\sigma^{-1}(i\omega_n)} = \frac{W_{\alpha s}}{\mathcal{G}_\sigma^{-1}(i\omega_n) - (J\sigma s + U)\alpha} - W_{\alpha s}G_\sigma(i\omega_n), \quad (25)$$

where

$$S_{n\sigma} = \sum_{\alpha s}\frac{W_{\alpha s}}{\left[\mathcal{G}_\sigma^{-1}(i\omega_n) - (J\sigma s + U)\alpha\right]^2}. \quad (26)$$

In such a way, Eqs. (19)–(25) fully determine the static magnetic susceptibility function in Eq. (17), once the self-consistent equations of the DMFT are solved. The static magnetic susceptibility diverges indicating the instability of the PM state. The $\mathbf{q}$ dependence of the susceptibility comes entirely from the bare susceptibility $\chi_0(\mathbf{q}, i\omega_n)$. To study the instability of the FM state one considers the uniform zone center point $\mathbf{q} = \mathbf{0}$, and the corresponding bare susceptibility reads [17]

$$\chi_0(\mathbf{0}, i\omega_n) = 2[1 - (i\omega_n + \mu - \Sigma_\sigma(i\omega_n))G_\sigma(i\omega_n)]. \quad (27)$$

Note here that the bare susceptibility is spin-independent because it is valid only in PM state. The single-particle Green function and its self-energy, in this case, do not depend on spin.

IV. NUMERICAL RESULTS

In this section, we present the numerical results analyzing the magnetic properties in the DMS in a compact theory. In doing so, we solve self-consistently the set of Eqs. (3), (9), and (12). In the calculation, the chemical potential μ is adjusted for a given value of the carrier density $n = n_\uparrow + n_\downarrow$, with $n_\sigma = \int d\omega A_\sigma(\omega)f(\omega)$, where $A_\sigma(\omega)$ and $f(\omega)$ are respectively the DOS of the itinerant carriers with spin σ and the Fermi-Dirac distribution function $f(\omega) = 1/(1 + e^{\beta\omega})$, $\beta = 1/T$ is inverse of temperature. The DOS is evaluated straightforwardly from its Green's function via $A_\sigma(\omega) = -\mathrm{Im}G_\sigma(\omega)/\pi$. Due to the heavy compensation in almost DMS systems, we use $n < x \ll 1$ [7,12]. To proceed with the task in the real frequency ω, we use the analytical continuation by replacing $i\omega_n = \omega + i0^+$, all summations of the Masubara frequencies, for instance, in Eq. (11) thus would be changed to integrals of the real frequency [15,17]. In the unit of the hoping integral, the magnetic coupling J in the present work is chosen in the range of 0–3, which is relevant to the implication of almost DMSs [57–60]. In our knowledge, the value of U relevant to the experimental observations is not clear. However, U in the work is chosen around the limitation at which the impurity band and the main band are separated.

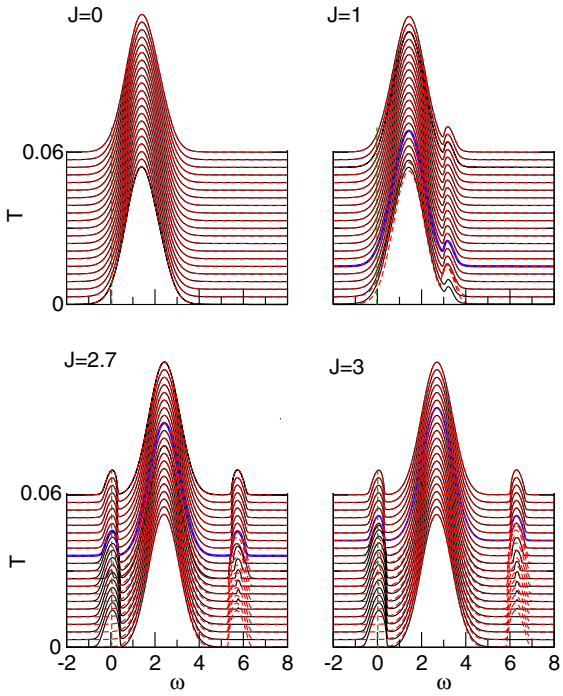

FIG. 1. Temperature dependence of the DOS $A_\sigma(\omega)$ ($\sigma =\uparrow$-black solid lines and $\sigma =\downarrow$-red dashed lines) of the itiernant carriers for different magnetic coupling J at $U = 0.5$, $n = 0.05$, and $x = 0.1$. Blue solid lines indicate the DOS at the FM-PM transition temperature and the green dashed line indicates the Fermi level.

A. Density of states

First of all, we discuss the magnetic properties of the DMS systems by analyzing the DOS $A_\sigma(\omega)$ of the itinerant carriers. Signature of the DOS of the itinerant carrier with different spin polarization could address the main points of the magnetic properties in the systems. In the FM state, DOSs of the spin-up and spin-down itinerant carriers below the Fermi level are not identical. In the meanwhile, they are the same in the PM state. In Fig. 1, we show the temperature dependent DOS of the itinerant carriers for different magnetic couplings J at $U = 0.5$ for $n = 0.05$ and $x = 0.1$. Without the magnetic coupling between the itinerant carrier and Mn ion ($J = 0$), apparently, the DOSs of spin-up (majority spin) and spin-down (minority spin) itinerant carriers are completely identical at all temperature. The system in this case, thus settles in the PM state. In this case, one finds no impurity band. At $J = 1$, the impurity band is still not isolated from the main band, however, in this case, one can find a difference between the signatures of the minority and majority spin DOSs at low temperature (lines below the solid blue line). The system thus settles in the FM state at low temperature and in the PM state at large temperature. The blue solid line indicates the DOS at the FM-PM transition temperature. Increasing temperature up to that transition temperature, two minority and majority spin DOSs of the itinerant carriers begin to merge with each other. At $J = 2.7$, the impurity band is separated from the main band. In this case, the discrepancy between the DOSs of different spins at low temperature has been transparently viewed. The FM-PM transition temperature at $J = 2.7$ has been increased up to $T \sim 0.035$. Increasing the magnetic coupling to $J = 3$, the impurity band is completely separated from the main band. At $T \to 0$, therefore, only majority spin carriers exist below the Fermi level. In this case, all impurity spins are aligned, say, in the z direction and the system settles in a saturated FM state. The FM-PM transition temperature, in this large J, is also increased to a temperature $T \sim 0.04$. For $n = x/2$, the Fermi level settles nearly at the middle of the impurity band at large magnetic coupling.

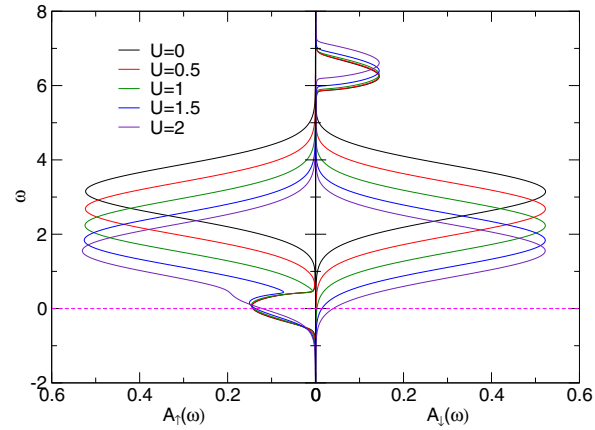

FIG. 2. Zero-temperature DOS $A_\sigma(\omega)$ of the itinerant carriers at different disorder U for $J = 3$, $n = 0.05$, and $x = 0.1$. The magenta dashed line indicates the Fermi energy.

Discussing effects of the disorder strength in the association of the FM-PM transition, in Fig. 2, we show the DOSs of the spin-up and spin-down carriers with $J = 3$, $n = 0.05$, and $x = 0.1$ at zero temperature for different values of U. If there is no disorder scattering in the system or $U = 0$, the magnetic coupling $J = 3$ is large enough to create the impurity band separately from the main band as discussed above in Fig. 1. Once the disorder is included, the majority spin carriers with spin parallel to the local magnetic moment feel a potential $-J + U$ on each magnetic impurity site and the minority spin carriers feel a potential $J + U$ [7]. Increasing the disorder scattering, therefore, decreases the potential magnetic scattering of the majority spin carriers and increases that of the minority ones. As a consequence, with increasing U the impurity band of the majority spin carriers generally merges with the main band. A minority spin band below the Fermi level develops or the spin-down carrier density becomes comparable with the up-spin carriers leading to an unstable FM state.

As a function of the carrier density n, zero-temperature DOSs of the spin-up and spin-down carriers at $J = 3$, $U = 0.5$, and $x = 0.1$ are displayed in Fig. 3. With increasing carrier density, both DOSs of up and down spin carriers are shifted to the lower energy. Once $n < x$, there is no signature of the spin-down (minority spin) DOS below the Fermi level, whereas, a partial part of the impurity band of up-spin (majority spin) carrier DOS is filled, the system thus settles in the FM state. In contrast, for the filled impurity band, i.e., for $n = x$, the Fermi level settles inside the gap between the impurity band and the main band. Especially, in that case, the DOS of the majority spin carrier in the impurity band

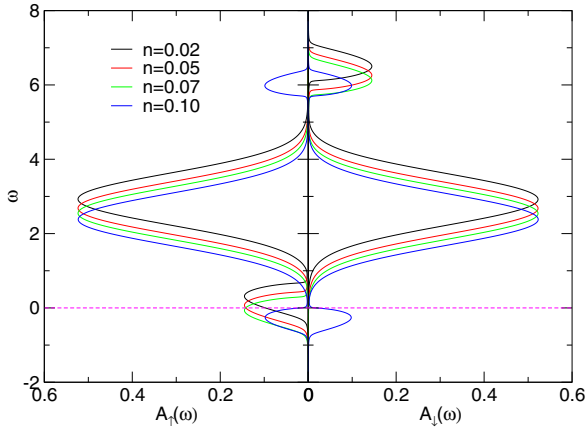

FIG. 3. Zero-temperature DOS $A_\sigma(\omega)$ of the itinerant carriers at different doping n for $J = 3$, $U = 0.5$, and $x = 0.1$. The magenta dashed line indicates the Fermi energy.

appears with the same spectral weight with the opposite one. In this case, no low energy hopping processes are allowed in the FM state, instead, only the antiferromagnetic (AFM) state hopping is favored. Competition between the FM and AFM is a fundamental and challenging problem of DMSs [5,61,62].

B. Self-energies

In the following, we discuss in more detail the spin dynamics properties in the system in a mention of the imaginary part of the self-energies. Understanding the self-energies might help us clear the nature of the quasiparticle excitation and different excitation states in both PM and FM states. In Fig. 4, we show the frequency dependence of the imaginary part $\mathrm{Im}\Sigma_\sigma(\omega)$ of the self-energies for different values of the magnetic coupling J at $U = 0.5$, $x = 0.1$, and $n = 0.05$ at zero temperature. In a free-magnetic scattering situation, i.e., $J = 0$, the imaginary parts of both majority spin $\mathrm{Im}\Sigma_\uparrow(\omega)$ and minority spin $\mathrm{Im}\Sigma_\downarrow(\omega)$ quasiparticles are identical, and in this case, the system settles in the PM state. Increasing the magnetic coupling, the peaks in the imaginary part of the self-energy of two opposite spin directions are separated,

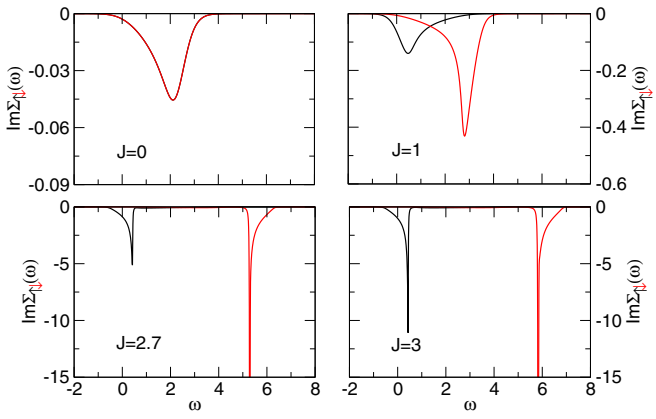

FIG. 4. The imaginary part of the zero temperature self-energies, $\mathrm{Im}\Sigma_\sigma(\omega)$, for different magnetic couplings J at $U = 0.5$, $x = 0.1$, and $n = 0.05$.

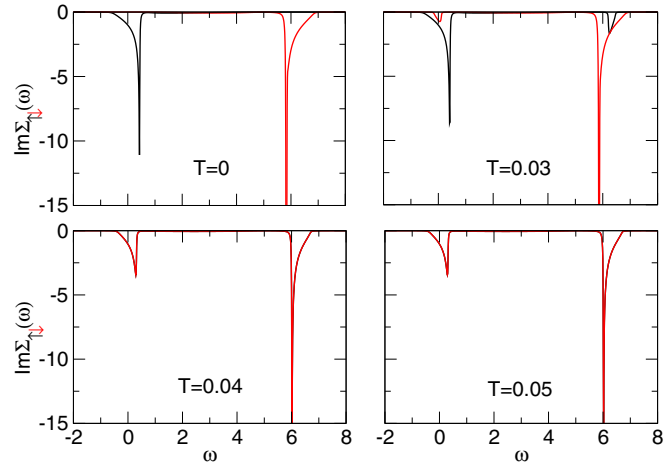

FIG. 5. Temperature dependence of the imaginary part of the self-energies, $\mathrm{Im}\Sigma_\sigma(\omega)$, for $J = 3$, $U = 0.5$ at $x = 0.1$ and $n = 0.05$.

that of the majority spin quasiparticle is shifted to the left, while that of minority spin quasiparticle is shifted to the right on the real-frequency axis. The system thus settles in the FM state. The shift is proportional with $2J$. Sharper peak in the self-energy of the minority spin carrier in comparison to that of the majority spin carriers is due to the displacement of the DOS of the former carriers to the high energies. In comparing with the DOS in Fig. 1, the gap between $\mathrm{Im}\Sigma_\downarrow(\omega)$ and $\mathrm{Im}\Sigma_\uparrow(\omega)$ indicates that there is no correlation scattering in the main-band, it is due to the semiconductor host. The correlations come from the quasiparticles in the impurity band only. At large enough J, one finds only nonzero of $\mathrm{Im}\Sigma_\uparrow(\omega)$ at the Fermi level or the system in a non-Fermi liquid of the spin-up quasiparticle.

Considering the Born approximation would lead to $\mathrm{Im}\Sigma \sim -xN(E_F)J^2$, where $N(E_F)$ is the DOS at the Fermi level [63]. With increasing magnetic coupling, a spin-polarized bound state can be formed for the majority spin leading to a strong increase of the effective magnetic scattering rate. In contrast, increasing J leads to an antibound state for the minority spin carrier and its effective scattering rate is thus decreased. The spin-polarized bound state of the quasiparticles in the impurity band is also indicated in a sharp signature of the self-energies [64]. The sharp peak of the self-energies remains in the whole temperature range as shown in Fig. 5. With increasing temperature, the thermal fluctuation excites the minority spin carriers, the correlation of the minority spin carriers individually contributes besides that of the majority spin carrier. At temperature close to the FM-PM transition point, the self-energies of both carriers with opposite spin directions merge with each other.

C. Magnetization and static magnetic susceptibility

To detect the FM state and the spin fluctuations in the FM state in a more explicit way, we discuss in the following the properties of magnetization. The magnetization is defined as $m = n_\uparrow - n_\downarrow$, where n_σ is the density of the spin σ carriers. In Fig. 6, we illustrate the magnetization m as a function of

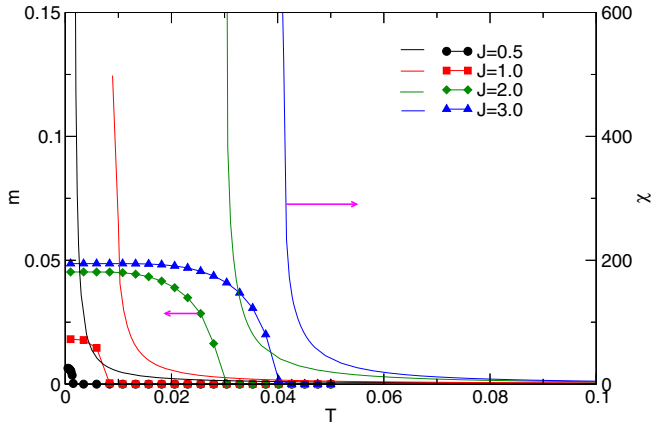

FIG. 6. Magnetization m (solid lines with symbols) and static magnetic susceptibility χ (solid lines) as functions of the temperature for different values of J at $U = 0.5$, $x = 0.1$, and $n = 0.05$.

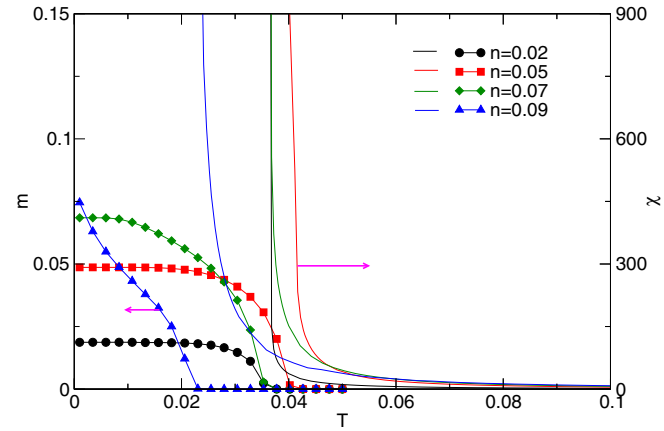

FIG. 7. Magnetization m (solid lines with symbols) and static magnetic susceptibility χ (solid lines) as functions of temperature for some values of n at $J = 3$, $U = 0.5$, and $x = 0.1$.

temperature in the case of $x = 0.1$, $n = 0.05$, and $U = 0.5$ for different values of magnetic coupling J. For all magnetic couplings ($J \geqslant 0.5$), the magnetization is finite at low temperature, indicating that the system stabilizes in the FM state. Increasing temperature, the spin of the carrier fluctuates and one finds with more probability the minority spin carriers below the Fermi level (cf. Fig. 1). The magnetization is thus depressed. If the temperature is larger than a so-called critical value T_c, the magnetization completely disappears and the system is in the PM state. The T_c, therefore, indicates the FM-PM transition or the Curie temperature. Increasing the magnetic coupling, the magnetization increases, and the Curie temperature increases as well. In case of large magnetic coupling ($J = 3$ for instance), the magnetization at very low temperature approaches the value of carrier density (in Fig. 6, that value is 0.05). Due to the large magnetic coupling, spins of all carriers are aligned in the direction of the impurity spin. Enlarging more the magnetic coupling thus does not affect the magnetization or the system stabilizes in the saturated FM state.

The magnetization, however, only shows us the spin dynamics properties in the FM state. To understand the spin dynamic properties also in the PM state, one needs to show the spin susceptibility function. Figure 6 shows the spin susceptibility χ as a function of temperature for the same set parameters in discussing the magnetization. As a function of temperature, the spin susceptibility behaves like the Curie-Weiss law, $\chi \sim 1/(T - T_c)$, i.e., the susceptibility in the PM state is diverging if the temperature reaches the PM-FM transition temperature. At a given magnetic coupling, rapid enhancement of spin susceptibility with reducing temperature close to the critical temperature indicates the development of spin fluctuations with decreasing temperature. In the meanwhile, at a given large temperature ensuring that the system settles in the PM state, increasing the magnetic coupling, the spin susceptibility increases. At low carrier density, it is suitable that in the PM state the magnetic scattering resolves the electronic mean free path l, satisfying the relationship $J \sim l \sim T\chi$ [30,33]. Increasing the magnetic coupling, therefore, provides a strong evidence that spin fluctuations are enlarged in the temperature range.

Next, we discuss the spin dynamics under the influence of the carrier doping. In Fig. 7, we show the magnetization and the spin susceptibility as a function of temperature for different carrier densities n at large magnetic coupling $J = 3$, $U = 0.5$, and $x = 0.1$. As expected, at very low temperature, the magnetization is finite, indicating that the system stabilizes in the FM state. As discussed before, at large magnetic coupling, the impurity band is completely separated from the main band, increasing the carrier density leads to an increase of the majority spin carrier. Increasing carrier density, therefore, increases the magnetization. In the whole temperature range, however, it is correct only with small n. In the case with large carrier densities $n \sim x$, one finds the opposite behavior of magnetization depending on temperature. Indeed, with enlarging n, the magnetization decreases if the temperature is increased, corresponding to a decreasing PM-FM transition temperature. In the limit of filled impurity band, i.e., $n = x$, no low-energy hopping processes are allowed in the FM state, instead, this case favors the AFM state hopping [5].

The dependence of the spin susceptibility on the temperature, in this case, is similar to that discussed previously in Fig. 6. However, as varying the carrier density, the behavior of the spin susceptibility becomes more complicated depending on temperature. At large temperature, the susceptibility increases with increasing carrier density indicating that the spin fluctuations in the system are enhanced if the carrier doping is enlarged. If the temperature approaches the critical value of PM-FM transition, one finds another scenario of the spin dynamics. At this range of temperatures, of course, the spin fluctuation is found to dominate at half impurity band filling, i.e., $n = 0.05$. In this case, the magnetic scattering is the largest. Deviating carrier density from this situation leads to suppressed spin fluctuations, as indicated by a decrease of the spin susceptibility.

D. Phase diagram of the FM-PM transition

From the discussion above in Fig. 6 and 7, the critical temperature of the PM-FM transition T_c can be determined either by a divergence of the spin susceptibility χ or by a vanishing condition of the magnetization m. We use here the former way

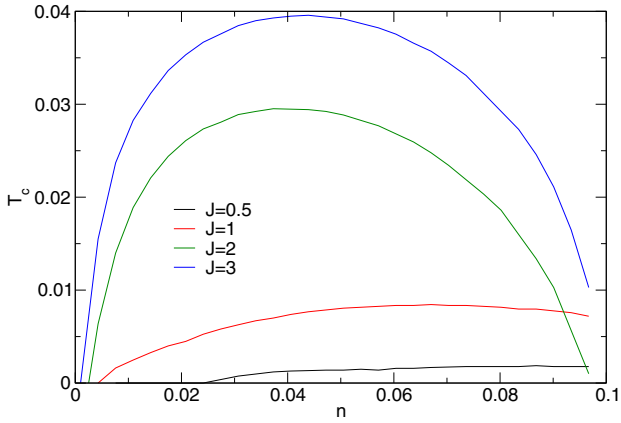

FIG. 8. PM-FM transition temperature T_c vs the itinerant carrier density n for different values of J at $U = 0.5$ and $x = 0.1$.

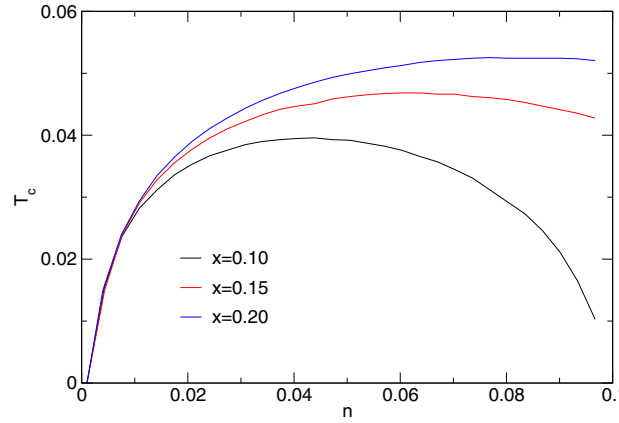

FIG. 9. PM-FM transition temperature T_c vs the itinerant carrier density n for some values of x at $J = 3$ and $U = 0.5$.

to evaluate the T_c. Figure 8 displays the PM-FM transition temperature T_c versus carrier density n for some different values of magnetic coupling J at $x = 0.1$ and $U = 0.5$. There are two opposite behaviors of T_c as a function of n at two different ranges of the magnetic coupling. At small magnetic coupling ($J \leqslant 1$), the impurity band either is not formed or not clearly formed (cf. Fig. 1), then the magnetic transition temperature increases with increasing carrier density over $n = x/2$. Otherwise, an impurity band is distinctly formed in the case of large magnetic coupling and one finds a nonmonotonic behavior of T_c. However, in this case, T_c becomes maximum at $n < x/2$. In the case of infinite magnetic coupling, i.e., $J \to \infty$, T_c is expected to become maximum at $n = x/2$. Because of the infinite magnetic coupling, the FM state is driven by the kinetic energy of the majority carriers only, and T_c would have been maximum in case of the electron-hole symmetry situation occurring in the impurity band. Noting here that the FM state is driven by the delocalization energy in the impurity band, and as a consequence, T_c diminishes at $n \to 0$ or $n \to x$. Once the impurity band is partly filled ($n \ll x$), the carrier is essential to launch the coupling between the spin of the carrier and the impurity magnetic moment. In this case, the FM-PM transition temperature increases with increasing magnetic coupling J. In contrast, for a nearly filled impurity band ($n \sim x$) situation, with increasing magnetic coupling, the carriers get more trapped in the spin impurity site. As a consequence, the mobility of the carriers is reduced and thus the magnetism is suppressed. If the impurity band is completely filled ($n = x$), only AFM state hoping is allowed and the ground state of the system is AFM state [5]. Studying a competition between the FM and AFM states in the DMS would be a worthwhile subject in the near future.

To discuss the impurity doping effect on the PM-FM transition in DMS, we present in Fig. 9 the PM-FM transition temperature as a function of the carrier density for different impurity dopings x at $U = 0.5$ and large magnetic coupling $J = 3$. At a given impurity doping, the behavior of the critical temperature dependence on the carrier density has been discussed before in Fig. 8. At a given carrier density, Fig. 9 shows us that the critical temperature increases with increasing impurity doping x. That signature can be understood if one notes here that the magnetic coupling between the carriers and impurity magnetic moment J is only efficient at the impurity sites. So for a given magnetic coupling, the effective coupling strength of the system increases with increasing impurity concentration x [65]. Moreover, increasing x, the impurity band is enlarged and the situation of the particle-hole symmetry occurs when $n \sim x/2$ takes place at a respectively large value of n. The maximum of T_c discussed previously in Fig. 8, therefore, shifts to a larger carrier density range.

In Fig. 10, we discuss the FM-PM transition in the system in the T-U plane for some different magnetic couplings J at $x = 0.1$ and $n = 0.05$. As discussed before in Fig. 2, switching on the disorder suppresses the magnetic potential of the majority spin carriers, otherwise, enhances that of the minority spin carriers. As a result, the FM state is diminished once the disorder increases. That scenario has been displayed in Fig. 10 at a given magnetic coupling J, where by increasing U, T_c is monotonically suppressed and if U is large enough, the system would be stabilized in the PM state even at zero temperature. To discuss the validity of the Ising approximation, we compare the critical temperature released in the present work with that reported in the literature. At $n = 0.02$ and $x = 0.1$ for $U = 0$ and $J = 1$, the red line in

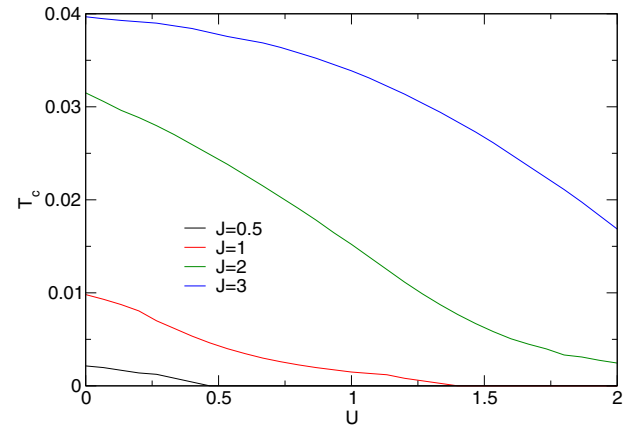

FIG. 10. PM-FM transition temperature T_c vs disorder strength U for different values of J at $x = 0.1$ and $n = 0.05$.

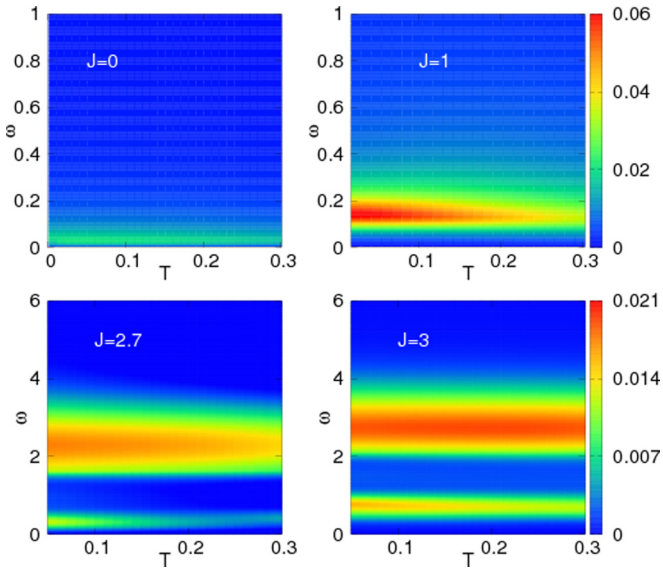

FIG. 11. Intensity plots of the imaginary part of the B_{1g} channel Raman scattering, $\mathrm{Im}\chi_{B1g}(\omega)$, at some values of J for $U = 0.5$, $x = 0.1$, and $n = 0.05$.

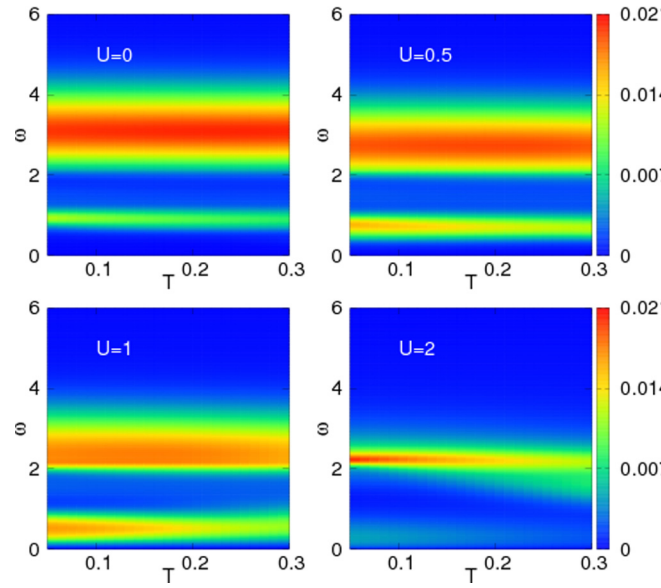

FIG. 12. Intensity plots of the imaginary part of the B_{1g} channel Raman scattering, $\mathrm{Im}\chi_{B1g}(\omega)$, at some values of U for $J = 3$, $x = 0.1$, and $n = 0.05$.

Fig. 10 gives T_c approximately equal to 0.01. This value is close to the critical temperature found in the same set of parameters once the localized spin is considered classically [5]. The Ising approach in the present calculation is thus not much exaggerated in evaluating the critical temperatures.

E. Raman scattering

To understand more about the spin fluctuations in the PM state in DMSs, in the remainder of this paper we discuss the electronic Raman scattering at a temperature above T_c for the Hamiltonian given in Eq. (1). In the B_{1g} channel, the nonresonant Raman response has no vertex corrections and in the infinite dimensional limitation, its imaginary part reads [37,38]

$$\mathrm{Im}\chi_{B1g}(\omega) = \pi \int d\nu \int d\varepsilon \rho(\varepsilon)[f(\nu) - f(\nu+\omega)] \times A(\varepsilon,\nu)A(\varepsilon,\nu+\omega), \quad (28)$$

where $A(\varepsilon,\nu)$ is a spectral function of the itinerant carriers. Here, we have assumed that the system is in the PM state and the carriers with different spins are homogenous, i.e.,

$$A(\varepsilon,\nu) = A_\sigma(\varepsilon,\nu) = -\frac{1}{\pi}\mathrm{Im}\frac{1}{\nu - \varepsilon + \mu - \Sigma_\sigma(\nu)}. \quad (29)$$

Here, the local self-energy $\Sigma_\sigma(\nu)$ has been determined in the framework of the DMFT in Sec. II.

Figure 11 displays the imaginary part of the Raman scattering $\mathrm{Im}\chi_{B1g}(\omega)$ depending on temperature T for some different values of magnetic coupling J at $U = 0.5$, $x = 0.1$, and $n = 0.05$. Once the magnetic coupling is small and the impurity band is not separated from the main band, i.e., at $J \leqslant 1$ (cf. Fig. 1), one finds only a single peak in the B_{1g} channel of the nonresonant Raman response (see upper panels in Fig. 11). At zero magnetic coupling ($J = 0$), there is no magnetic ordered state in the system even at zero temperature. The Raman scattering response, therefore, releases a weak signature near zero frequency, indicating a weak spin fluctuation in the PM state. Increasing the magnetic coupling, the amplitude of the peak increases at a larger frequency, the spin fluctuations thus become stronger. The pronounced peak indicates that the magnetic polarons form in the PM state. In the situation with the completely formed impurity band, i.e., at large magnetic coupling, one finds a two-peak structure in the B_{1g} spectral signatures (see lower panels in Fig. 11). A low-frequency peak identifies the magnetic polaron formation arising from the impurity band, whereas, a large frequency peak indicates a quasiparticle excitation arising from the main band. Increasing the magnetic coupling, the low-frequency peak shifts up in the energy. The magnetic polaron is favored by the large magnetic coupling between the carrier and the impurity magnetic moment. That magnetic coupling causes a trapped charge to lower its energy by polarizing the local moments. In all cases, the peak frequency is temperature independent, however, its amplitude is decreased or the magnetic polaron signature is smeared out with increasing temperature. The behavior of the electronic Raman response is similar to that observed in the t-J model by using the finite-temperature diagonalization method [66] or in the Hubbard model by using the cluster DMFT [67] at low doping. Our theoretical results are also in agreement with the observations of the magnetic polaron formation observed in PM state in some low doping ferromagnetic semiconductors [30].

Lastly, to discuss the disorder effect on the electronic Raman response in the systems, we show in Fig. 12 the B_{1g} channel spectral signatures in the dependence of temperature at different disorder U for $J = 3$, $x = 0.1$, and $n = 0.05$. Once the disorder is small (see upper panels in Fig. 12), one finds a sharp peak at low frequency, indicating signatures of the magnetic polaron formation. The feature remains if U is increased up to $U = 1$. Increasing the disorder, therefore,

the peak at low-frequency shifts down in the energy with a bit smeared out spectral weight. In particular, at $U = 2$, the low-frequency response is nearly depleted, indicating that the magnetic polaron has been diminished. The disorder, in this case, becomes a point that depletes the magnetic order state as discussed before. At given disorder strength and magnetic coupling, the B_{1g} channel spectral signature always falls off with increasing temperature indicating that with the appearance of the thermal fluctuations, the magnetic polaron and also the spin fluctuations are depressed. In the contrast, for $T \to T_c$, the enhancement of carrier scattering by spin fluctuations with the development of magnetic polarons leads the system to the a FM ordered state if $T < T_c$. These results illustrate that the electronic Raman scattering can probe the spin dynamics properties in paramagnetic diluted magnetic semiconductors.

V. CONCLUSION

In summary, we have investigated the magnetic properties in diluted magnetic semiconductors in the entire range of temperatures in a compact theory. In doing so, the dynamical mean-field theory has been adapted to the Kondo lattice model including lightly random magnetic impurity distribution. In the infinite dimensional limit, we have derived a set of self-consistent equations allowing us to evaluate the single-particle Green functions. The static magnetic susceptibility and then the B_{1g} channel Raman response expressions are obtained. At low temperature, by analyzing the itinerant carrier density of states and magnetization, we have indicated a stability of the ferromagnetic state. Increasing temperature, the thermal fluctuations diminish the ordered state and the system favors a paramagnetic state. Phase diagrams showing the ferromagnetic-paramagnetic transition temperature T_c depending on the model parameters then have been constructed. The spin fluctuation scenario in the paramagnetic state has been pointed out in the signatures of the self-energies, the static magnetic susceptibility, and the Raman scattering. Analyzing the properties of the B_{1g} channel Raman response, we have attributed the formation of magnetic polarons in the paramagnetic state. Our results thus illustrate that the electronic Raman scattering can probe the spin dynamics properties with the formation of magnetic polarons in the disordered paramagnetic state in diluted magnetic semiconductors. The magnetic polaron scenario in diluted magnetic semiconductors, therefore, is discussed based on the dynamical mean-field approach. Moreover, the paramagnetic-ferromagnetic transition in the system in the signature of the static magnetic susceptibility function is also addressed in the same framework. The competition of the ferromagnetic and antiferromagnetic states at low temperature and the formation of magnetic polarons leading the system to an antiferromagnetic state if the temperature is smaller than the Neel temperature in DMSs are also important and will be considered in the near future.

ACKNOWLEDGMENT

This research is funded by the Vietnam National Foundation for Science and Technology Development (NAFOSTED) under Grant No. 103.01-2017.68.

[1] T. Jungwirth, J. Wunderlich, V. Novák, K. Olejník, B. L. Gallagher, R. P. Campion, K. W. Edmonds, A. W. Rushforth, A. J. Ferguson, and P. Němec, Rev. Mod. Phys. **86**, 855 (2014).
[2] T. Dietl and H. Ohno, Rev. Mod. Phys. **86**, 187 (2014).
[3] O. M. Fedorych, E. M. Hankiewicz, Z. Wilamowski, and J. Sadowski, Phys. Rev. B **66**, 045201 (2002).
[4] T. Dietl, H. Ohno, F. Matsukura, J. Cibert, and D. Ferrand, Science **287**, 1019 (2000).
[5] A. Chattopadhyay, S. Das Sarma, and A. J. Millis, Phys. Rev. Lett. **87**, 227202 (2001).
[6] G. Alvarez, M. Mayr, and E. Dagotto, Phys. Rev. Lett. **89**, 277202 (2002).
[7] E. H. Hwang and S. Das Sarma, Phys. Rev. B **72**, 035210 (2005).
[8] A. Kaminski, V. M. Galitski, and S. Das Sarma, Phys. Rev. B **70**, 115216 (2004).
[9] J. Schliemann and A. H. MacDonald, Phys. Rev. Lett. **88**, 137201 (2002).
[10] A. Kaminski and S. Das Sarma, Phys. Rev. Lett. **88**, 247202 (2002).
[11] A. Kaminski and S. Das Sarma, Phys. Rev. B **68**, 235210 (2003).
[12] S. Das Sarma, E. H. Hwang, and A. Kaminski, Phys. Rev. B **67**, 155201 (2003).
[13] V. M. Galitski, A. Kaminski, and S. Das Sarma, Phys. Rev. Lett. **92**, 177203 (2004).
[14] F. Popescu, Y. Yildirim, G. Alvarez, A. Moreo, and E. Dagotto, Phys. Rev. B **73**, 075206 (2006).
[15] A. Georges, G. Kotliar, W. Krauth, and M. J. Rozenberg, Rev. Mod. Phys. **68**, 13 (1996).
[16] D.-H. Bui and V.-N. Phan, Ann. Phys. **375**, 313 (2016).
[17] J. K. Freericks and V. Zlatić, Rev. Mod. Phys. **75**, 1333 (2003).
[18] A. C. Durst, R. N. Bhatt, and P. A. Wolff, Phys. Rev. B **65**, 235205 (2002).
[19] A. J. Millis, R. Mueller, and B. I. Shraiman, Phys. Rev. B **54**, 5389 (1996).
[20] A. J. Millis, R. Mueller, and B. I. Shraiman, Phys. Rev. B **54**, 5405 (1996).
[21] S. Ciuchi and F. de Pasquale, Phys. Rev. B **59**, 5431 (1999).
[22] S. Ciuchi, F. de Pasquale, and D. Feinberg, Europhys. Lett. **30**, 151 (1995).
[23] S. Ciuchi and S. Fratini, Phys. Rev. B **77**, 205127 (2008).
[24] E. Cappelluti and S. Ciuchi, Phys. Rev. B **66**, 165102 (2002).
[25] E. Cappelluti, S. Ciuchi, and S. Fratini, Phys. Rev. B **76**, 125111 (2007).
[26] E. Cappelluti, S. Ciuchi, and S. Fratini, Phys. Rev. B **79**, 012502 (2009).
[27] P. Nyhus, S. Yoon, M. Kauffman, S. L. Cooper, Z. Fisk, and J. Sarrao, Phys. Rev. B **56**, 2717 (1997).
[28] H. L. Liu, S. Yoon, S. L. Cooper, S.-W. Cheong, P. D. Han, and D. A. Payne, Phys. Rev. B **58**, R10115 (1998).

[29] S. Yoon, H. L. Liu, G. Schollerer, S. L. Cooper, P. D. Han, D. A. Payne, S.-W. Cheong, and Z. Fisk, Phys. Rev. B **58**, 2795 (1998).
[30] C. S. Snow, S. L. Cooper, D. P. Young, Z. Fisk, A. Comment, and J.-P. Ansermet, Phys. Rev. B **64**, 174412 (2001).
[31] M. Nawrocki, R. Planel, G. Fishman, and R. Galazka, Phys. Rev. Lett. **46**, 735 (1981).
[32] T. Dietl and J. Spałek, Phys. Rev. Lett. **48**, 355 (1982).
[33] T. Dietl and J. Spałek, Phys. Rev. B **28**, 1548 (1983).
[34] M. Umehara, Phys. Rev. B **61**, 12209 (2000).
[35] I. A. Akimov, M. Salewski, I. V. Kalitukha, S. V. Poltavtsev, J. Debus, D. Kudlacik, V. F. Sapega, N. E. Kopteva, E. Kirstein, E. A. Zhukov *et al.*, Phys. Rev. B **96**, 184412 (2017).
[36] E. A. Zhukov, Y. G. Kusrayev, K. V. Kavokin, D. R. Yakovlev, J. Debus, A. Schwan, I. A. Akimov, G. Karczewski, T. Wojtowicz, J. Kossut *et al.*, Phys. Rev. B **93**, 245305 (2016).
[37] J. K. Freericks, T. P. Devereaux, and R. Bulla, Phys. Rev. B **64**, 233114 (2001).
[38] J. K. Freericks and T. P. Devereaux, Phys. Rev. B **64**, 125110 (2001).
[39] M. Berciu and R. N. Bhatt, Phys. Rev. Lett. **87**, 107203 (2001).
[40] T. Jungwirth, J. Sinova, J. Mašek, J. Kučera, and A. H. MacDonald, Rev. Mod. Phys. **78**, 809 (2006).
[41] T. Minh-Tien, Phys. Rev. B **67**, 144404 (2003).
[42] B. M. Letfulov and J. K. Freericks, Phys. Rev. B **64**, 174409 (2001).
[43] V.-N. Phan and M.-T. Tran, Phys. Rev. B **72**, 214418 (2005).
[44] V.-N. Phan, Q.-H. Ninh, and M.-T. Tran, Phys. Rev. B **93**, 165115 (2016).
[45] V.-N. Phan and M.-T. Tran, Phys. Rev. B **92**, 155201 (2015).
[46] K. Kagami, M. Takahashi, and K. Kubo, J. Supercond. **18**, 121 (2005).
[47] K. Kagami, M. Takahashi, C. Yasuda, and K. Kubo, Sci. Technol. Adv. Mater. **7**, 31 (2006).
[48] M. Takahashi, Materials **3**, 3740 (2010).
[49] V. Janiš and D. Vollhardt, Phys. Rev. B **46**, 15712 (1992).
[50] R. Strack and D. Vollhardt, Phys. Rev. B **46**, 13852 (1992).
[51] R. Vlaming and D. Vollhardt, Phys. Rev. B **45**, 4637 (1992).
[52] V. Janiš, M. Ulmke, and D. Vollhardt, Europhys. Lett. **24**, 287 (1993).
[53] M. Ulmke, V. Janiš, and D. Vollhardt, Phys. Rev. B **51**, 10411 (1995).
[54] U. Brandt and C. Mielsch, Z. Phys. B **75**, 365 (1986).
[55] U. Brandt and C. Mielsch, Z. Phys. B **79**, 295 (1990).
[56] U. Brandt and C. Mielsch, Z. Phys. B **82**, 37 (1991).
[57] J. Okabayashi, A. Kimura, O. Rader, T. Mizokawa, A. Fujimori, T. Hayashi, and M. Tanaka, Phys. Rev. B **58**, R4211 (1998).
[58] F. Matsukura, H. Ohno, A. Shen, and Y. Sugawara, Phys. Rev. B **57**, R2037 (1998).
[59] M. Abolfath, T. Jungwirth, J. Brum, and A. H. MacDonald, Phys. Rev. B **63**, 054418 (2001).
[60] Y. Yildirim, Ph.D. thesis, Florida State University, 2007.
[61] S. J. Pearton, C. R. Abernathy, G. T. Thaler, R. M. Frazier, D. P. Norton, F. Ren, Y. D. Park, J. M. Zavada, I. A. Buyanova, W. M. Chen *et al.*, J. Phys. Condens. Matter **16**, R209 (2004).
[62] S. Dhar, O. Brandt, A. Trampert, K. J. Friedland, Y. J. Sun, and K. H. Ploog, Phys. Rev. B **67**, 165205 (2003).
[63] E. H. Hwang, A. J. Millis, and S. Das Sarma, Phys. Rev. B **65**, 233206 (2002).
[64] S. Biermann, L. de' Medici, and A. Georges, Phys. Rev. Lett. **95**, 206401 (2005).
[65] K. Pradhan and S. K. Das, Sci. Rep. **7**, 8 (2017).
[66] P. Prelovšek and J. Jaklič, Phys. Rev. B **53**, 15095 (1996).
[67] N. Lin, E. Gull, and A. J. Millis, Phys. Rev. Lett. **109**, 106401 (2012).